The "Mirror" Estimate: An Intuitive Predictor of Membrane Polarization during Extracellular Stimulation

Sébastien Joucla and Blaise Yvert*
CNRS, Université de Bordeaux, UMR5228, Bordeaux, F-33000 France

ABSTRACT Achieving controlled extracellular microstimulation of the central nervous system requires understanding the membrane response of a neuron to an applied electric field. The "activating function" has been proposed as an intuitive predictor of membrane polarization during stimulation, but subsequent literature raised several limitations of this estimate. In this study, we show that, depending on the space constant λ, the steady-state solution to the passive cable equation is theoretically well approximated by either the activating function when λ is small, or the "mirror" image of the extracellular potential when λ is large. Using simulations, we then explore the respective domain of both estimates as a function of λ, stimulus duration, fiber length, and electrode-fiber distance. For realistic λ ($>$50–100 μm), the mirror estimate is the best predictor for either long electrode-fiber distances or short distances ($<$20–30 μm) when stimulus durations exceed a few tens of microseconds. For intermediate distances, the mirror estimate is all the more valid that the stimulus duration is long and the fiber is short. We also illustrate that this estimate correctly predicts the steady-state membrane polarization of complex central nervous system arborizations. In conclusion, the mirror estimate can often be preferred to the activating function to intuitively predict membrane polarization during extracellular stimulation.

INTRODUCTION

Extracellular electrical stimulation of excitable tissues has been used empirically for decades, both with fundamental and clinical goals. New advances in microelectrode arrays allowing to interface large neural networks with hundreds of recording and stimulating sites have triggered a strong enthusiasm in finding pertinent paradigms of extracellular microstimulation to modify, and even control, the dynamics and plasticity of neural networks. To address this question, the first step is to understand the direct effect of an extracellular stimulation on the membrane response of a single cell within the tissue. In this respect, many studies have been carried out to highlight the effect of electric and magnetic stimulations on the membrane polarization of excitable cells (1–31). Simulation approaches require the calculation of 1), the potential field generated in the tissue by a stimulus; and 2), the membrane response of the cell to this potential field. The first computation of the potential field can be done either analytically in simple geometrical cases (32–34) or numerically for more realistic geometries (30,35–37). This study will focus on the second computation, namely the prediction of membrane polarization from a known potential field. Originally, a cable equation formalism was proposed by McNeal (2) and further extended by Rattay (3). These pioneering works have shown that the temporal and spatial variations of the membrane potential are driven by an equation (see Eq. 2), the source term of which is proportional to the second derivative of the extracellular potential field along the fiber, and called the ''activating function''. The activating function has then been considered as a predictor of the subthreshold membrane polarization at the beginning of a stimulation (3,5,20). The advantage of this approach is to provide a simple and intuitive estimate of excitation and inhibition sites along the fiber, without requiring a full knowledge of biophysical properties of the cell. However, subsequent studies (8,12,15,38,39) have pointed out several limitations of the activating function in being an accurate predictor of the membrane polarization. This is due to the importance of longitudinal currents that are neglected when considering the activating function as the solution to the cable equation, and to boundary fields playing an important role at the fiber terminations. These limitations come from the fact that, although the activating function drives the cable equation, this quantity is not usually the solution to this equation, except far from the edges (hence for sufficiently long fibers) and at the stimulus onset when longitudinal currents have no strong influence.

In this study, we show that a very simple analytical steady-state solution to the cable equation can often be used as an alternative to the activating function to intuitively estimate the membrane potential of a finite fiber in response to an extracellular potential field. This estimate is given by the opposite of the extracellular potential field, centered on its spatial mean value along the fiber, and will thus be referred to as the ''mirror'' estimate. In a first step, we show that, theoretically, the steady-state membrane profile depends strongly on the fiber space constant: the membrane voltage is best reflected either by the activating function for ''small enough'' space constants, or by the mirror solution for ''large enough'' space constants. In a second step, by solving numerically the cable equation, we examine the domains—in terms of space constants, stimulation durations, fiber lengths, and electrode-fiber distances—where either the mirror or the activating function estimates are most adequate.

Submitted June 4, 2008, and accepted for publication December 15, 2008.

*Correspondence: b.yvert@cnic.u-bordeaux1.fr

Editor: Michael D. Stern.

0006-3495/09/05/3495/14 $2.00

doi: 10.1016/j.bpj.2008.12.3961

We show that the mirror domain includes a wide range of these parameters encountered in practice, and that this simple analytical estimate can often be used advantageously in practice to intuitively predict the response of a finite fiber as well as complex neuronal structures subject to extracellular stimulation.

THEORETICAL BACKGROUND

We derive the steady-state solution to the cable equation for a passive uniform unmyelinated fiber of finite length L, compartmentalized in $N+1$ segments ($k=0\ldots N$, Fig. 1). Table 1 summarizes the meaning of each variable used in this study. Each compartment is modeled by an equivalent electrical circuit representing both the membrane and the intracellular medium. The classic cable equation is obtained by applying Kirchhoff's Current Law, at a given node k, which expresses that the sum of currents flowing through the membrane equals the sum of intracellular currents.

Cable equation within the fiber

Within the fiber, at any node k in $1\ldots N-1$, this law leads to the following relation:

$$C_{\mathrm{m}}^{(k)} \times \frac{d\left(V_{\mathrm{int}}^{(k)} - V_{\mathrm{ext}}^{(k)}\right)}{dt} + G_{\mathrm{l}}^{(k)} \times \left(V_{\mathrm{int}}^{(k)} - V_{\mathrm{ext}}^{(k)} - V_{\mathrm{r}}\right) = \frac{V_{\mathrm{int}}^{(k-1)} - V_{\mathrm{int}}^{(k)}}{R^{(k,k-1)}} + \frac{V_{\mathrm{int}}^{(k+1)} - V_{\mathrm{int}}^{(k)}}{R^{(k,k+1)}}, \quad (1)$$

where $V_{\mathrm{int}}^{(k)}$ and $V_{\mathrm{ext}}^{(k)}$ stand for the intra- and extracellular potentials, respectively, $C_{\mathrm{m}}^{(k)}$ for the membrane capacitance, $G_{\mathrm{l}}{}^{(k)}$ for the leakage conductance, and $R^{(k,k+1)}$ for the resistance between compartments k and $k+1$. For a uniform fiber, as considered in this study, these membrane parameters are identical for all compartments k, and can be expressed as functions of surface and linear quantities: $C_{\mathrm{m}} = c_{\mathrm{m}} \times \pi \times d \times \Delta s$, $G_{\mathrm{l}} = g_{\mathrm{l}} \times \pi \times d \times \Delta s$, $R = \rho_{\mathrm{i}} \times 4 \times \Delta s/(\pi \times d^2)$.

By considering the reduced membrane potential (i.e., the variations of the membrane potential around its resting value) $V_{\mathrm{m}} = V_{\mathrm{int}} - V_{\mathrm{ext}} - V_{\mathrm{r}}$, and defining the membrane time constant $\tau = c_{\mathrm{m}}/g_{\mathrm{l}}$ and the fiber space constant $\lambda = [d/(4 \times \rho_{\mathrm{i}} \times g_{\mathrm{l}})]^{1/2}$, Eq. 1 becomes:

$$\tau \times \frac{dV_{\mathrm{m}}^{(k)}}{dt} + V_{\mathrm{m}}^{(k)} - \lambda^2 \times \frac{V_{\mathrm{m}}^{(k-1)} - 2 \times V_{\mathrm{m}}^{(k)} + V_{\mathrm{m}}^{(k+1)}}{\Delta s^2} = \lambda^2 \times \frac{V_{\mathrm{ext}}^{(k-1)} - 2 \times V_{\mathrm{ext}}^{(k)} + V_{\mathrm{ext}}^{(k+1)}}{\Delta s^2} \quad (k = 1\ldots N-1). \quad (2)$$

Equation 2 shows that, within the fiber, the membrane potential is the solution of a set of ordinary differential equations whose source term (on the right-hand side) is proportional to the discrete second derivative of the extracellular potential in the direction of the fiber. Following the definition of Rattay (5), this source term will be referred to as activating function and noted f_{a} in the following.

Boundary equations

In the case of a finite fiber, Eq. 2 should be modified at the fiber terminations. A common assumption is that the ends of the fiber are ''sealed'' so that no axial current exit the fiber from compartments $k = 0$ and $k = N$ (8,16,40). This assumption leads to the following boundary equations:

$$\begin{aligned} \tau \times \frac{dV_{\mathrm{m}}^{(0)}}{dt} + V_{\mathrm{m}}^{(0)} - \lambda^2 \times \frac{-V_{\mathrm{m}}^{(0)} + V_{\mathrm{m}}^{(1)}}{\Delta s^2} &= \lambda^2 \times \frac{-V_{\mathrm{ext}}^{(0)} + V_{\mathrm{ext}}^{(1)}}{\Delta s^2} \quad (k = 0), \\ \tau \times \frac{dV_{\mathrm{m}}^{(N)}}{dt} + V_{\mathrm{m}}^{(N)} - \lambda^2 \times \frac{-V_{\mathrm{m}}^{(N)} + V_{\mathrm{m}}^{(N-1)}}{\Delta s^2} &= \lambda^2 \times \frac{-V_{\mathrm{ext}}^{(N)} + V_{\mathrm{ext}}^{(N-1)}}{\Delta s^2} \quad (k = N). \end{aligned} \quad (3)$$

Equation 3 shows that, at the sealed ends, the source term is not related to the second, but to the first difference of the extracellular potential. For this reason, the response of a finite fiber is likely to be different from that of an infinite fiber.

Steady-state solution

At the steady state of the stimulation, when the membrane potential does not vary anymore with time, the capacitive

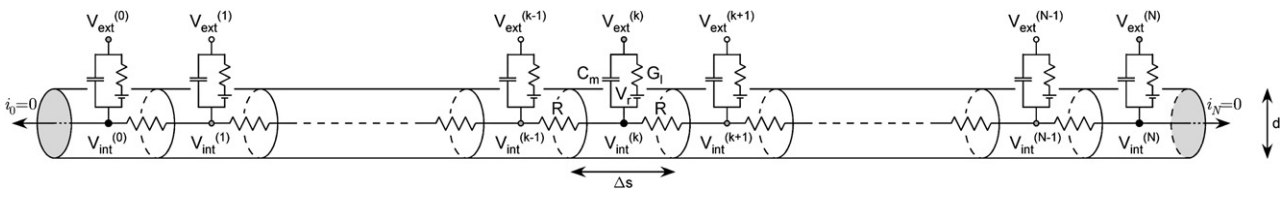

FIGURE 1 Schematic cable representation of the uniform passive fiber used in this study. The fiber is divided in $N+1$ compartments of equal length Δs, each of which is modeled by an equivalent circuit consisting of a capacitance C_{m} in parallel with a leakage conductance G_{l} (in series with the resting potential V_{r}). Each compartment connects its neighbors through an intracellular resistance R. The fiber is sealed at its terminations, so that no longitudinal current exit the fiber at compartments 0 and N. V_{int} and V_{ext} stand for the intracellular and extracellular potentials, respectively.

TABLE 1 Symbols and terms used in this study

Symbol	Definition	Usual unit
C_{fa}	Matching criterion between the membrane potential and the activating function estimate	No dimension (within [−1,1])
c_m	Surface membrane capacitance	$\mu F/cm^2$
C_m	Compartment membrane capacitance	μF
C_{mirror}	Matching criterion between the membrane potential and the mirror estimate	No dimension (within [−1,1])
d	Fiber diameter	μm
D	Electrode-fiber distance	μm
Δs	Compartment length	μm
E	Electric field	mV/mm
f_a	Activating function ($= \lambda^2 \times \partial^2 V_{ext}/\partial s^2$)	mV
g_l	Surface leakage conductance	S/cm^2
G_l	Compartment leakage conductance	S
I	Current injected through the stimulation electrode	μA
k	Compartment number	No dimension
L	Fiber length	μm
λ	Fiber space constant ($= [d/(4 \times \rho_i \times g_l)]^{1/2}$)	μm
λ_f	λ value at the frontier between the f_a domain and the mirror domain	μm
mirror	Opposite of the extracellular potential ($-V_{ext}$) centered on its spatial mean ($\langle V_{ext} \rangle$)	mV
$N + 1$	Number of compartments	No dimension
r	Electrode-compartment distance	μm
R, $R^{(k)}$	Compartment intracellular resistance	Ω
$R^{(k,k+1)}$	Intercompartment resistance ($= [R^{(k)} + R^{(k+1)}]/2$)	Ω
R_{fa}	Amplitude ratio between the membrane potential and the activating function, at the center of the fiber	No dimension (within [0,1])
R_{mirror}	Amplitude ratio between the membrane potential and the mirror, at the center of the fiber	No dimension (within [0,1])
ρ_i	Intracellular medium resistivity	$\Omega \times cm$
s	Axial coordinate along the fiber	μm
σ	Extracellular medium conductivity	S/m
t	Time	μs
τ	Fiber membrane time constant ($= c_m/g_l$)	μs
V_{ext}	Extracellular potential	mV
$\langle V_{ext} \rangle$	Mean of the extracellular potential along the fiber	mV
V_{int}	Intracellular potential	mV
V_m	Reduced membrane potential ($= V_{int} - V_{ext} - V_r$)	mV
V_r	Membrane resting potential	mV

term can be dropped, and the system of Eqs. 2 and 3 depends only on the fiber space constant λ:

$$V_m^{(k)} - \lambda^2 \times \frac{V_m^{(k-1)} - 2 \times V_m^{(k)} + V_m^{(k+1)}}{\Delta s^2} = \lambda^2 \times \frac{V_{ext}^{(k-1)} - 2 \times V_{ext}^{(k)} + V_{ext}^{(k+1)}}{\Delta s^2}, \quad (4a)$$

$$V_m^{(0)} - \lambda^2 \times \frac{-V_m^{(0)} + V_m^{(1)}}{\Delta s^2} = \lambda^2 \times \frac{-V_{ext}^{(0)} + V_{ext}^{(1)}}{\Delta s^2}, \quad (4b)$$

$$V_m^{(N)} - \lambda^2 \times \frac{-V_m^{(N)} + V_m^{(N-1)}}{\Delta s^2} = \lambda^2 \times \frac{-V_{ext}^{(N)} + V_{ext}^{(N-1)}}{\Delta s^2}. \quad (4c)$$

In general, except for very simple geometrical configurations, there are no analytical solutions to these equations. However, we can consider two cases for which a general analytical solution exists, corresponding to either λ small enough or λ large enough, respectively.

Case 1: small enough space constant λ (the activating function estimate)

For small values of λ, the V_m spatial derivative terms in the left-hand side of Eq. 4a–c can be neglected compared with the V_m term. In this case, the profile of V_m directly follows that of the source term f_a, within the fiber. At the fiber terminations, the membrane potential is driven by the first difference of the extracellular potential. In the case of high V_{ext} gradients, the resulting V_m response at the fiber ends will greatly differ from that within the fiber. By definition of the space constant λ, the boundary behavior of the fiber will not affect the V_m profile on more than a few λ (typically <5). Hence, in this case, the steady-state solution, away from the terminals, corresponds to the classical activating function, which has usually been considered to depict the initial membrane polarization at the onset of the stimulation (3).

Case 2: large enough space constant λ (the mirror estimate)

Conversely, for high values of λ, the V_m spatial derivative terms in Eq. 4 become preponderant and the V_m term can be dropped. In this case, the system of Eq. 4 becomes:

$$V_m^{(k-1)} - 2 \times V_m^{(k)} + V_m^{(k+1)} = -V_{ext}^{(k-1)} + 2 \times V_{ext}^{(k)} - V_{ext}^{(k+1)}, \quad (5a)$$

$$-V_m^{(0)} + V_m^{(1)} = V_{ext}^{(0)} - V_{ext}^{(1)}, \quad (5b)$$

$$-V_m^{(N)} + V_m^{(N-1)} = V_{ext}^{(N)} - V_{ext}^{(N-1)}. \quad (5c)$$

A trivial solution of Eq. 5a is:

$$V_m^{(k)} = -V_{ext}^{(k)} + c_1 \times k \times \Delta s + c_2. \quad (6)$$

Contrary to Case 1, because λ is high, the boundary conditions significantly affect the whole fiber response. Indeed, introducing Eq. 6 into boundary Eq. 5b or Eq. 5c leads to $c_1 \times \Delta s = 0$, and thus, $c_1 = 0$. Moreover, summing all Eqs. 4 leads to:

$$\sum_{k=0}^{N} V_m^{(k)} = 0, \quad (7)$$

irrespective of the value of λ. This equation reflects the fact that all current flowing into the neuron must flow out. By combining Eqs. 6 and 7, we show that the constant c_2 equals the mean value of the extracellular potential field along the fiber. Finally, the complete expression of V_m becomes:

$$V_m^{(k)} = -V_{ext}^{(k)} + \frac{1}{N+1}\sum_{j=0}^{N} V_{ext}^{(j)} = -V_{ext}^{(k)} + \langle V_{ext}\rangle. \quad (8)$$

For a continuous fiber of length L, this expression becomes:

$$V_m(s) = -V_{ext}(s) + \frac{1}{L}\int_{s=-L/2}^{L/2} V_{ext}(s)\,ds = -V_{ext}(s) + \langle V_{ext}\rangle. \quad (9)$$

This simple steady-state expression of V_m shows that for sufficiently long space constants, the response of the fiber is the mirror of the extracellular potential field, centered on its mean value along the fiber. Determining zones of depolarization and hyperpolarization of the membrane using Eq. 9 then becomes intuitive, for only the knowledge of V_{ext}—and not that of its spatial derivatives—is necessary. Note that, in this case, the intracellular potential across all compartments is the same and equals the mean extracellular potential.

Extension to neurons

The mirror concept derived above for unmyelinated uniform fibers can be extended to neurons presenting branching points or nonuniformity in diameter, leakage conductance density, or intracellular resistivity.

At a branching point k, with neighbors k_0, k_1, and k_2, Eq. 4a is indeed modified as:

$$V_m^{(k)} - \lambda^2 \times \frac{V_m^{(k_0)} - 3\times V_m^{(k)} + V_m^{(k_1)} + V_m^{(k_2)}}{\Delta s^2} = \lambda^2 \times \frac{V_{ext}^{(k_0)} - 3\times V_{ext}^{(k)} + V_{ext}^{(k_1)} + V_{ext}^{(k_2)}}{\Delta s^2}, \quad (10)$$

and, with the same approach as above, we can show that the mirror Eq. 8 remains valid.

In the case of a nonuniform fiber or neuron, λ differs from one compartment to another, and it can be shown (see Appendix) that the membrane potential is the mirror of the extracellular potential centered on its mean value along the fiber weighted by the inverse of λ^2:

$$V_m(s) = -V_{ext}(s) + \frac{\int_{s=-\frac{L}{2}}^{\frac{L}{2}} V_{ext}(s)/\lambda(s)^2 ds}{\int_{s=-\frac{L}{2}}^{\frac{L}{2}} 1/\lambda(s)^2 ds}. \quad (11)$$

This latter expression should be used for instance when taking into account the cell body with a larger diameter or when the distribution of leakage conductance is nonuniform over the neuron.

From these formulations, we thus predict that the value of the space constant of the fiber (that ranges typically from 100 to 2000 μm in practice) strongly influences which estimate (activating function or mirror) best predicts the membrane polarization at the steady state of an extracellular stimulation.

METHODS

Using numerical simulations, we examined the respective domain of validity of each estimate in the case of a passive unmyelinated fiber, in terms of space constant values and stimulation durations. We also determined how the fiber length and the electrode-fiber distance alter these domains. We finally tested the validity of either estimate in the case of two realistic central nervous system (CNS) neurons. The system of Eqs. 2 and 3 was solved using the NEURON software, v6.1 (41).

Passive unmyelinated fiber

Unless otherwise stated, simulations were carried out with a reference configuration consisting of a 1-μm diameter and 1000-μm-long sealed-end fiber, with the center located 10 μm from a point-source stimulation electrode (Fig. 2). The fiber was uniformly discretized in compartments of equal length. Each compartment was assigned identical electrical characteristics: the surface capacitance was set to its classical value ($c_m = 1$ μF/cm^2), the intracellular resistivity was set to $\rho_i = 100\,\Omega \times$ cm, which is within the range 33–300 $\Omega \times$ cm of values used in the literature (19,21,25,31,42). We also tested the influence of the space constant value, the fiber length, and the electrode-fiber distance. When varying the space constant value, the value of the leakage surface conductance was adjusted to adapt to the desired value of λ ($g_l = d/(\lambda^2 \times 4 \times \rho_i)$).

Realistic neurons

We also tested the validity of the mirror estimate for two realistically reconstructed compartment models taken from the literature (43) and obtained from ModelDB (accession number 2488). One model corresponded to a neocortical stellate cell having a rather compact morphology (see Fig. 7 *A1*), whereas the other model corresponded to a pyramidal neuron having a more elongated arborization (see Fig. 7 *B1*). Because we focused on the passive responses of these cells to a stimulation, all original active conductances of these models were removed. The passive properties of these cells were left unchanged: $c_m = 0.75$ μF/cm^2, $g_l = 1/30{,}000$ S/cm^2, $\rho_i = 150\ \Omega \times$ cm. The average space constant values were 637 $\pm$ 161 μm (range, 353–3391 μm) for the stellate neuron and 653 $\pm$ 240 μm (range, 387–3536 μm) for the pyramidal cell.

Extracellular potential field

Unless otherwise stated, we considered a point-source electrode delivering a cathodic current ($I = -1$ μA) in the extracellular space, which was modeled as a uniform conductive medium ($\sigma = 0.3$ S/m). The resulting extracellular potential field, created at a distance r from the electrode, was thus given by the relation:

$$V_{ext}(r) = \frac{I}{4 \times \pi \times \sigma \times r}. \quad (12)$$

For each fiber compartment, the distance r was calculated between the location of the electrode (in front of the middle of the fiber) and the center of the compartment.

We also tested how the two estimates behave in the case of a uniform electric field ($E = -10$ mV/mm) oriented in the direction of the fiber (Fig. 2 *B*).

In the NEURON environment, the extracellular stimulation can be modeled either through the extracellular mechanism or through IClamp

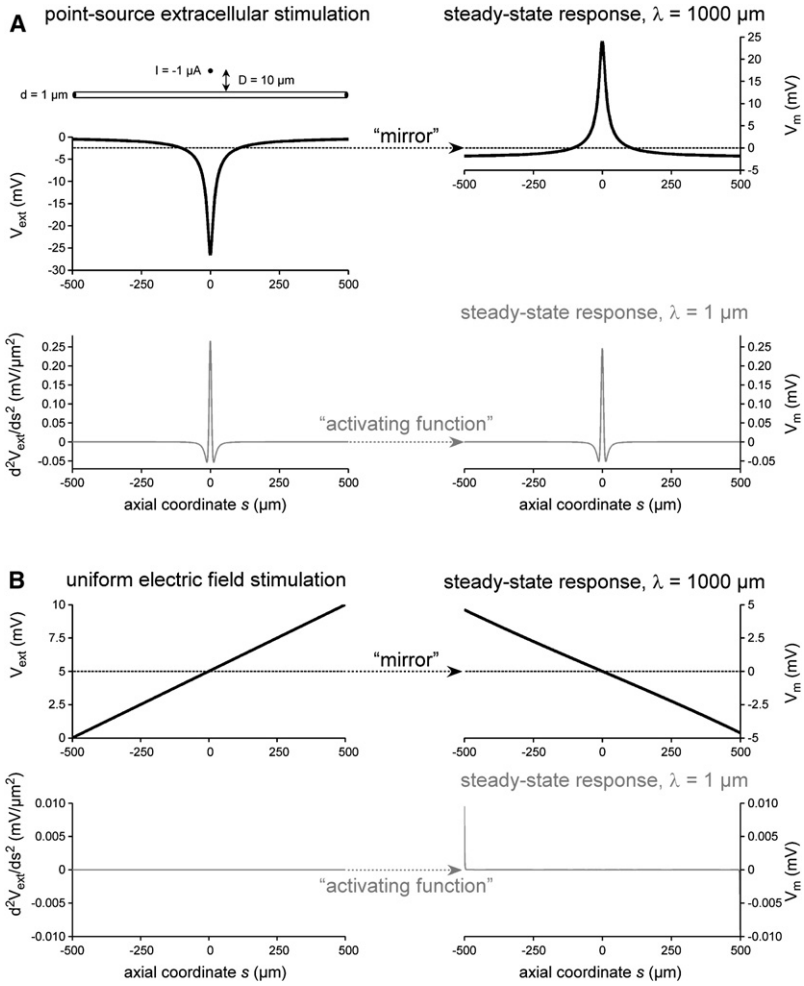

FIGURE 2 The steady-state response of a uniform passive fiber to an extracellular potential field depends on the space constant λ. (*A*) A $L = 1000$ μm-long fiber is stimulated by a cathodic point-source electrode located at $D = 10$ μm from its center. This stimulation induces a potential field V_{ext} in the extracellular medium (*left, top*), which second spatial derivative (*left, bottom*) determines the source term of the cable equation driving the fiber membrane potential. For $\lambda = 1$ μm, the steady-state membrane potential profile is close—in shape and amplitude—to that of the source term (activating function estimate). On the contrary, for $\lambda = 1000$ μm, the membrane potential is the exact opposite of the extracellular potential, centered on its spatial average (mirror estimate). (*B*) A $L = 1000$ μm-long fiber is stimulated by a uniform electric field $E = -10$ mV/mm parallel to the fiber. The induced extracellular potential field varies linearly along the fiber, and the activating function is zero. For $\lambda = 1$ μm, the steady-state membrane potential profile is also zero, except near the fiber terminations. Conversely, for $\lambda = 1000$ μm, the membrane potential varies linearly along the fiber, following the mirror estimate.

point processes. In the first case, the value of the extracellular potential corresponding to the compartment location is assigned at the center of the compartment. In the second case, the corresponding intracellular current is equal to the second finite difference of the extracellular potential, divided by the intercompartment resistance (see Eq. 1). We verified that both approaches gave identical results, and chose the second one because it allowed an easier use of adaptive time step integrators to solve the cable equation (see below). For the realistic simulations of Fig. 7, we used the extracellular mechanism with a fixed time step of 1 μs.

Stimulation time courses consisted of square pulse stimuli of different durations. Before the stimulation, the intracellular current, as well as the reduced membrane potential, was set to 0 for all compartments.

Numerical accuracy of the cable equation integration

The computational errors in the numerical resolution of the cable equation were minimized by choosing appropriate time and space discretization. The numerical errors arising from the time integration were optimized using the adaptive time scheme provided by NEURON (Cvode). In all simulations, we used the implicit backward Euler method (default, second order = 0). Regarding the spatial compartmentalization, we used a space step compatible with the steepness of the activating function (of the order of the micron) and adapted to the space constant λ and to the length L of the fiber: $\Delta s = \min(1, L/1000, \lambda/10)$. With this space- and time-discretization, the membrane potential differed by <1% from that computed with a twice finer compartmentalization and a 0.1-μs time step.

Evaluation of the estimates

To quantify the closeness of the membrane potential to either the activating function or the mirror of the extracellular potential, we calculated a matching quantity between the membrane potential profile and each of the estimates, both at the steady state and at different stimulation times. These matching criteria, referred to as C_{fa} and C_{mirror}, in the following, are defined as:

$$C_{fa} = \frac{\langle V_m, f_a \rangle}{\sqrt{\langle V_m, V_m \rangle \times \langle f_a, f_a \rangle}}, \tag{13a}$$

$$C_{mirror} = \frac{\langle V_m, mirror \rangle}{\sqrt{\langle V_m, V_m \rangle \times \langle mirror, mirror \rangle}}. \tag{13b}$$

A perfect match between an estimate and the membrane polarization would lead to $C = 1$. It should be noted that, when values are centered with respect to their mean, C equals the classical correlation. This is always verified for C_{mirror}, because the mirror estimate is centered (by definition) and so is the membrane polarization V_m (Eq. 7). By contrast, the activating function is not necessary centered and may even be unipolar over the whole fiber.

The best adequacy of either the activating function or the mirror estimate, was assessed by determining which estimate gave the highest matching criterion C. Although these criteria did not account for differences in amplitude, the estimate leading to the highest C best predicted the zones of depolarization and hyperpolarization of the fiber. Hence, when exploring different parameter values, the "domain" of an estimate was defined as the domain of parameters for which this estimate gave the highest C value.

We also assessed the accuracy of prediction of the membrane polarization amplitude. For this purpose, we computed the ratio between the membrane potential and each of the estimates at the center of the fiber, where the membrane polarization was maximal. These quantities are referred to as R_{fa} ($= V_m/f_a$) and R_{mirror} ($= V_m$/mirror), in the following.

RESULTS

We predicted that, at the steady state, the spatial distribution of the membrane potential would be related either to the activating function, or to the mirror of the extracellular electrical potential, depending on whether the fiber space constant λ was ''sufficiently low'' or ''sufficiently high''. As shown in Fig. 2 *A* for our reference fiber (1-mm long, 1-μm diameter, point source electrode at 10 μm), numerical simulations confirmed this prediction: although the membrane polarization follows the activating function when $\lambda = 1$ μm ($C_{fa} = 1.00$ and $R_{fa} = 0.93$, whereas $C_{mirror} = 0.33$ and $R_{mirror} = 0.01$), it is the exact mirror of the potential field when $\lambda = 1000$ μm ($C_{mirror} = 1.00$ and $R_{mirror} = 1.00$, whereas $C_{fa} = 0.33$ and $R_{fa} = 0.00009$). Consequently, the membrane potential profiles differ both in shape and amplitude, depending on the value of λ. In this example, when $\lambda = 1000$ μm, the mirror profile is much wider than the activating function one (the sites of hyperpolarization are different), and its amplitude at the peak is much higher (~100 times higher). In the case of the uniform electric field stimulation, illustrated in Fig. 2 *B*, similar results were obtained: For a small λ ($= 1$ μm), the best predictor is the activating function (that is zero), except near the ends of the fiber, where it fails to predict the very local hyperpolarization at one end and depolarization at the other end (these polarizations being due to the nonzero extracellular voltage gradient at the terminals). As λ increases, these terminal polarizations invade more and more the fiber, until the whole membrane polarization becomes linear from one end to the other. This situation is reached for $\lambda = 1000$ μm, in which case the mirror estimate gives an excellent prediction of the membrane polarization ($C_{mirror} = 1.00$).

We explore in more detail the domains where either the activating function or the mirror estimate is most adequate, in terms of λ values, stimulus durations, fiber lengths, and electrode-fiber distances.

Influence of the space constant λ

In Fig. 3, we further assess the influence of the fiber space constant on the adequacy between the steady-state V_m profile and either estimate. As shown in Fig. 3 *A*, the matching criterion C_{fa} decreases as the space constant of the fiber increases (*thin gray curve*). Conversely, C_{mirror} increases for increasing values of λ (*thick black curve*). In the case of our reference fiber, the activating function is a better predictor of the membrane polarization when $\lambda < 22$ μm, whereas for higher space constant values, the mirror estimate is more accurate. This frontier value $\lambda_f = 22$ μm thus separates the domains of validity of the activating function and of the mirror estimates.

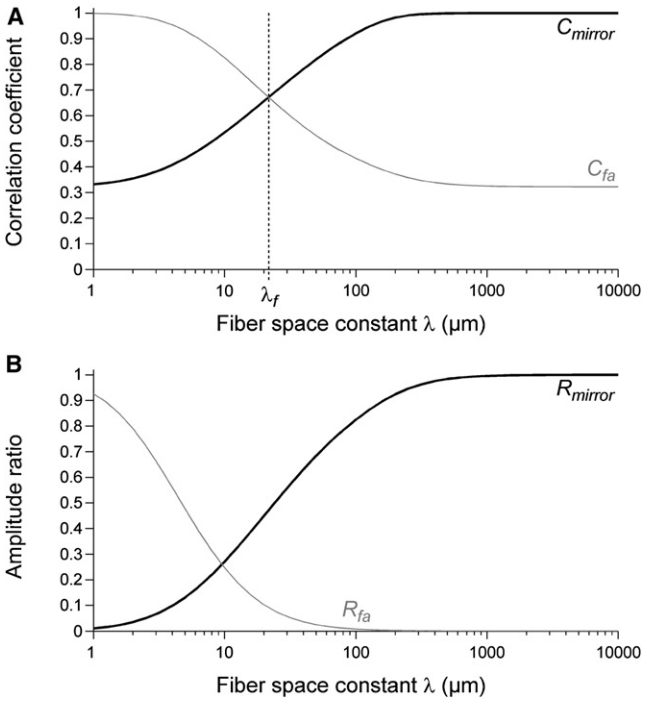

FIGURE 3 Influence of the fiber space constant on the best adequacy of either the activating function or the mirror estimates at the steady state ($L = 1000$ μm, $D = 10$ μm). The quality of the steady-state estimation of V_m by either f_a or the mirror of V_{ext} for the same configuration as in Fig. 2, is quantified by two criteria: (*A*) the matching criterion C between the profile of V_m and either estimate; and (*B*) the amplitude ratio R between V_m and either estimate, at the middle of the fiber. The domain of each estimate is defined as the range of λ values for which the matching criterion C of this estimate is the highest. The activating function estimate (*thin gray line*) is best for small space constants, whereas the mirror estimate (*thick black line*) is best for higher space constants. In this example, the frontier between the two domains corresponds to $\lambda_f = 22$ μm.

It should be noted that the matching criteria C_{fa} and C_{mirror} reflect shape similarities but do not account for any overall scaling ratio between the membrane potential and either estimates. We thus further determined the accuracy of the prediction of the membrane polarization amplitude (Fig. 3 *B*). Globally, a high matching criterion is accompanied by a high amplitude ratio and the monotony of the R_{fa} and R_{mirror} curves is identical to that of C_{fa} and C_{mirror}, respectively. In this example, the mirror estimate better predicts the amplitude of the membrane polarization for $\lambda > 10$ μm, this prediction overreaching 95% accuracy for $\lambda > 250$ μm.

In this study, our main interest was to quantify the global adequacy of the activating function and the mirror estimates with the membrane potential, which was better emphasized by a global measure taking into account the whole spatial response of the fiber, than by a local value of the membrane potential. Thus, we will only refer to the matching criteria C_{fa} and C_{mirror} to determine the respective domains of either estimate and to quantify how these domains vary as a function of the stimulus duration, the fiber length and the electrode-fiber distance.

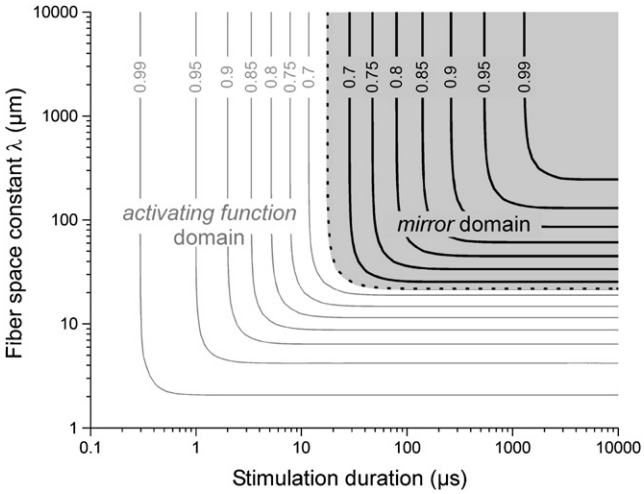

FIGURE 4 From the activating function to the mirror estimate: influence of the stimulation duration ($L = 1000\ \mu m$, $D = 10\ \mu m$). Isolines are plotted as a function of the stimulus duration and the fiber space constant. Matching criteria between V_m and f_a (*thin gray lines*) or between V_m and the mirror of V_{ext} (*thick black lines*) are shown, whichever is the highest. The gray dotted line shows the frontier between the activating function and the mirror domains (λ_f). The f_a domain is restricted to short stimulations or small space constants, whereas the mirror domain (*shaded area*) includes a large class of stimulation durations and fiber space constants encountered in practice.

Influence of the stimulus duration

The two estimates being steady-state solutions of the cable equation, they are theoretically valid only for infinitely long stimulations. However, in practice, stimulations have a finite duration. We thus determined the influence of the stimulation duration on the matching criteria $C_{fa}(\lambda)$ and $C_{mirror}(\lambda)$, as well as on the frontier value λ_f separating the activating function and mirror domains. This is illustrated in Fig. 4, which is an extension of Fig. 3 *A* for different stimulation durations. In Fig. 4, isolines represent isovalues of C_{fa} (*thin gray lines*) or C_{mirror} (*thick black lines*), whichever is higher for each given pair of values of λ and stimulation duration. The dotted line (on which $C_{fa} = C_{mirror}$) separates the domains where either the activating function or the mirror estimate was a best predictor. It thus represents how λ_f varies as a function of the stimulus duration. The mirror domain encompasses stimulations longer than 25 μs and space constant larger than 30 μm.

We have shown previously how the activating function and mirror domains evolved for different space constants and stimulation durations in the case of our reference fiber (1000-μm-long, located 10 μm from the point-source electrode). Below, we determine the influence of the fiber length and the electrode-fiber distance on these particular domains.

Influence of the fiber length

Fig. 5 *A* shows the influence of the fiber length on the respective validity of both the mirror and the activating function

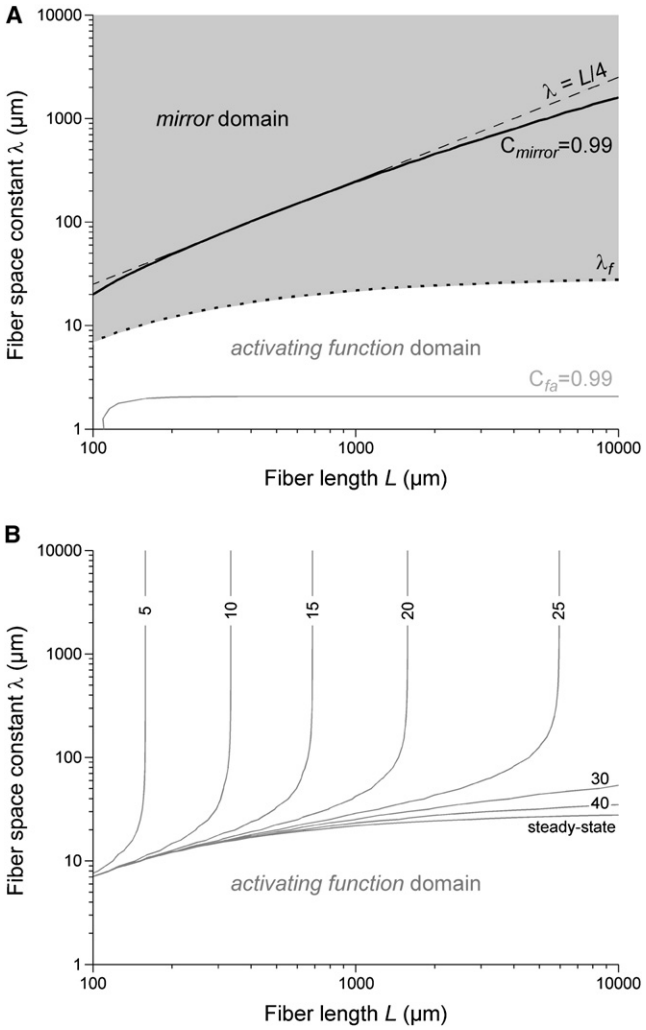

FIGURE 5 From the activating function to the mirror estimate: influence of the fiber length ($D = 10\ \mu m$). (*A*) Influence of the fiber length L on the f_a and mirror domains, at the steady state. The thin gray (*respectively thick black*) line corresponds to a matching criterion of 0.99 between V_m and f_a (respectively, the mirror of V_{ext}). The black dotted line in between delimits the frontier λ_f between both domains (the mirror domain is shaded). The matching criterion between V_m and the mirror estimate always exceeds 0.99 as long as $\lambda > L/4$ (*black dashed line*). (*B*) Time-dependent evolution of λ_f until the steady state is reached.

estimates at the steady state. Gray and black lines in Fig. 5 *A* represent 99% matching values for C_{fa} and C_{mirror}, respectively. It can be seen that 99% matching between V_m and the activating function is reached for small space constant values $\lambda < 2.2\ \mu m$ for any fiber length $>150\ \mu m$. By contrast, 99% matching between V_m and the mirror estimate is reached for values of λ that increase with the fiber length L. As a rule of thumb, 99% mirror matching is reached for $\lambda \sim L/4$ (Fig. 5 *A*, *black dashed line*). Moreover, the black dotted line in Fig. 5 *A* shows the frontier value λ_f separating the two domains as a function of the fiber length (the mirror domain is shaded). It can be seen that λ_f only slightly increases as the fiber length increases (from $\lambda = 7\ \mu m$ when $L = 100\ \mu m$ to $\lambda = 28\ \mu m$

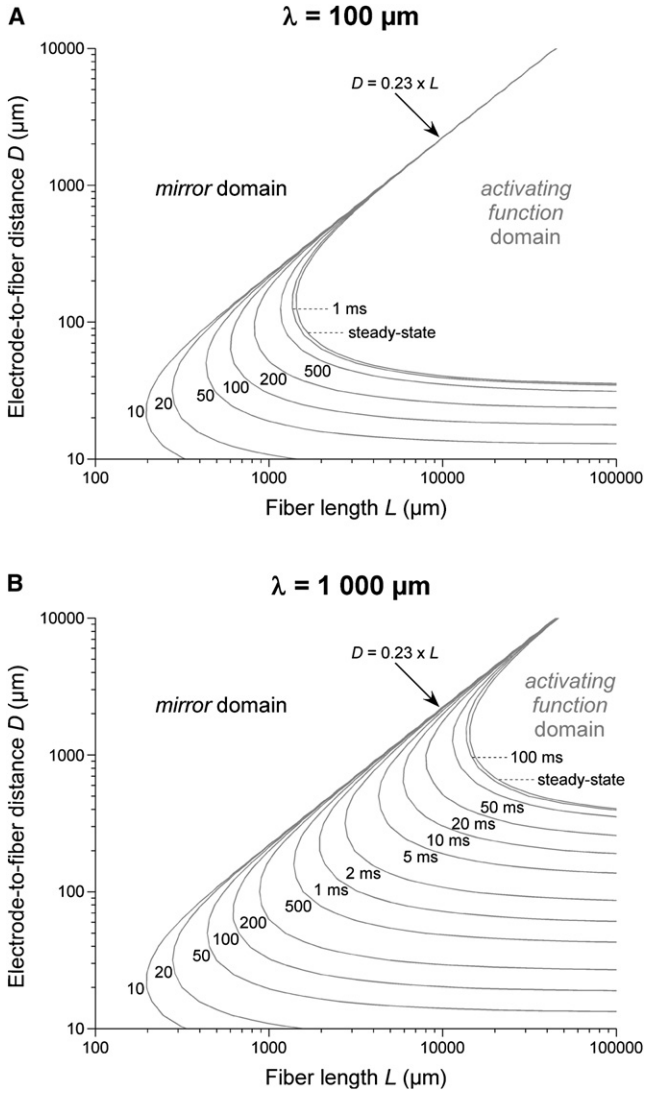

FIGURE 6 From the activating function to the mirror estimate: combined influence of the fiber length and electrode-fiber distance. The frontier between the mirror and the activating function domains is plotted as a function of the electrode-fiber distance and fiber length for different stimulus durations. Two different space constant values are considered, corresponding to typical values encountered in the literature: (*A*) 100 μm; (*B*) 1000 μm. The mirror domain encompasses both large (>0.23 $\times$ *L*) distances irrespective of the stimulus duration and the fiber length, and small (<20–30 μm) distances as long as the stimulus duration exceeds a few tens of microseconds. For a given fiber length, the activating function domain only encompasses a restricted range of intermediate distances, this range shrinking for increasing stimulus durations.

when $L = 10$ mm), and that the mirror estimate is a better predictor of the steady-state membrane potential when λ exceeds 28 μm.

These results were obtained by considering the membrane potential at the steady state, assuming a sufficiently long stimulus duration. We next evaluated how the λ_f-frontier varied with the stimulus duration. As shown in Fig. 5 *B*, this frontier remains similar to that obtained at the steady state, as long as the stimulus duration remains >30 μs. For smaller durations, the mirror domain shrinks to the left, meaning that this estimate remains a better predictor only for smaller fiber lengths (and $\lambda > 30$ μm).

Influence of the electrode-fiber distance

We also determined the influence of the electrode-fiber distance on the activating function and mirror domains (Fig. 6). For this purpose, the frontier between both domains was determined for different stimulus durations as a function of both the fiber length and the electrode-fiber distance. This was done for two given space constants corresponding to typical values encountered in the literature ($\lambda = 100$ μm in Fig. 6 *A* and $\lambda = 1000$ μm in Fig. 6 *B*).

We found that the mirror estimate was always the best predictor for large distances (>0.23 $\times$ *L*), irrespective of the stimulus duration and the space constant. The mirror estimate was also the best predictor for small electrode-fiber distances (<20–30 μm) even for very long fibers, provided that the stimulus duration exceeded a few tens of microseconds. For intermediate distances, the mirror estimate is all the more valid that the stimulus duration is long and the fiber length is small. For the example of 100-μs pulses (as often encountered in practice), the mirror estimate is a better predictor of the membrane potential than the activating function for fibers having lengths up to 600 μm, irrespective of the electrode-fiber distance, whereas for longer fibers, there is a restricted range of distances for which the activating function is the best predictor. For longer pulses, the mirror domain extends to longer fibers. Moreover, it might be worth noting that for very long stimulations (several ms), the domain of the activating function dramatically shrinks when the space constant is high (Fig. 6 *B*). Also, by comparing Fig. 6, *A* and *B*, it can be seen that when $\lambda = 1000$ μm, the time needed to reach the steady-state domain frontier for long fibers is much longer (~100 ms) than when $\lambda = 100$ μm (~1 ms). This is due to the fact that increasing λ is achieved by decreasing the surface leakage conductance, hence increasing the membrane time constant.

Case of realistic geometries

We finally verified that the mirror estimate can indeed be used to predict membrane polarization of the whole arborization of realistically reconstructed passive cortical neurons (Fig. 7). We tested the case of a compact stellate cell (Fig. 7 *A1*) and that of a more elongated pyramidal cell (Fig. 7 *B1*). Fig. 7, *A2* and *B2*, illustrate, for each cell, the extracellular voltage (top) and the steady-state membrane polarization (*bottom*), for all the compartments. As further illustrated in Fig. 7, *A3* and *B3*, the steady-state polarization of the neuron closely matched the mirror estimate in both cases ($C_{mirror} = 1.00$ for the stellate cell, and $C_{mirror} = 0.97$ for the pyramidal cell). We checked that considering the sodium and potassium voltage-dependent conductances at rest would have decreased the compartments' space constants by <10%, and thus would

not have strongly changed these results. We also found that the steady state was reached faster for the compact arborization (C_{mirror} reaches 0.99 in ~2.5 ms) than for the elongated one (C_{mirror} reaches 0.96 in ~25 ms). The evolution of the matching quantity C_{mirror} with time shows that the mirror estimate is a better predictor of the membrane polarization than the activating function for stimulus durations >10 μs for the compact stellate neuron and 22 μs for the larger pyramidal cell (Fig. 7, *A4* and *B4*).

DISCUSSION

Since the pioneering works of McNeal (2) and Rattay (3,5), the activating function has become a widely accepted predictor of membrane polarization for neurons or fibers subject to an extracellular electric or magnetic stimulation, and has been validated on numerical simulations (20). Hence, the results of this study (showing that the mirror estimate is a better predictor of membrane polarization than the activating function in several cases) may seem contradictory with the literature.

However, other previous studies have already pointed out that the activating function could not explain the membrane polarization in all cases (8,38). The limitations of this estimate stem from two facts. First, the activating function is really the source term that drives the temporal evolution of the membrane potential, but is generally not itself the solution to the cable equation. Hence, except at the very beginning of the stimulation (when intracellular currents are small compared with membrane currents) or for extremely (and unrealistically) small space constants (Figs. 2–5), the membrane potential cannot generally be approximated by the activating function source term (12). In the case of infinite fibers, V_m should actually be considered as a low-pass-filtered image of this quantity (39). Second, in the practical case of finite structures, boundary source terms are not related to the activating function but to the gradients of the extracellular field, which can greatly modify the fiber response (8,15). For instance, linear potential fields have been shown theoretically (8) and experimentally (38) to be able to depolarize finite fibers, although the activating function is zero in this case. This is due to the fact that the boundary source terms are not equal to zero (Fig. 2 *B*).

To overcome these limitations, an alternative is to derive analytical solutions to the cable equation (4,7,18,39). However, this can only be achieved in cases of particular geometries, and such solutions become often non intuitive. Hence, although modifications of the activating function have also been derived (12,44), no general and intuitive estimate of the solution to the cable equation has been proposed so far as an alternative to the activating function concept.

In this study, we proposed a simple estimate of membrane polarization of a finite fiber during an extracellular stimulation, called mirror estimate. Considering finite unmyelinated passive fibers, we theoretically showed that, depending on the fiber space constant λ, the steady-state membrane polarization was best predicted either by the activating function (when λ is small) or by the mirror estimate (when λ is large). The derivation of the analytical expression of the mirror solution, which is given by the opposite of the extracellular potential centered on its mean spatial value, is based on Eq. 7, which in turn stems from the choice of sealed-end boundary conditions. This choice, which is the one made in most theoretical and numerical studies, has been shown by Rubinstein (16) to be adequate for high space constants.

Following Eq. 9, the mirror estimate is theoretically valid for any extracellular potential field. It applies especially in the case of a uniform electric field E oriented in the direction of the fiber, which creates a linear potential field (Fig. 2 *B*). This is apparently in contradiction with a result of Coburn (6) reporting that the terminal polarizations of a fiber in the case of uniform field E are given by $\pm E \times \lambda$. By contrast, the mirror estimate suggests that the terminal polarizations be independent of λ. We thus checked the evolution of the terminal polarization as a function of λ in the case of our 1-mm-long fiber (data not shown). We found that the terminal polarization indeed linearly increases with λ for values of λ smaller than ~200 μm, but that for higher values, the amplitude of the polarization stagnates to $E \times L/2$ and no longer depends on λ. Thus, this linear relation does not apply for large space constants (i.e., when the mirror estimate applies). It should also be noted that in this case of a uniform field, the analytical mirror formulation simplifies to: $V_m(s) = E \times s$ for $-L/2 \leq s \leq L/2$.

An interesting feature of the membrane polarization during stimulation is given by Eq. 7: the average polarization along the fiber is zero. As a consequence, an electrical stimulation always creates zones of depolarization and hyperpolarization. This is also what the mirror estimate predicts, because this quantity is by definition centered with respect to its mean over the morphology. By contrast, the activating function is not generally centered, and may even be unipolar along the whole fiber, for example predicting a global depolarization of the whole fiber. This is especially the case for electrode-to-fiber distances above 0.70 times the fiber length, for which the activating function will always fail to predict zones of depolarization and hyperpolarization.

Given the two steady-state analytical estimates, our main goal was to determine numerically their respective domain of validity. For a point-source electrode located at 10 μm from the fiber, the frontier value λ_f between both domains was of the order of 20 μm (Fig. 3), and this was almost independent of the fiber lengths considered in this study, provided that the stimulation duration was >~30 μs (Fig. 5). It is interesting to note that, depending on the type of tissue, typical space constant values for unmyelinated fibers are within the range of 100–2000 μm (21,31,45,46), which should thus make the mirror estimate generally valid

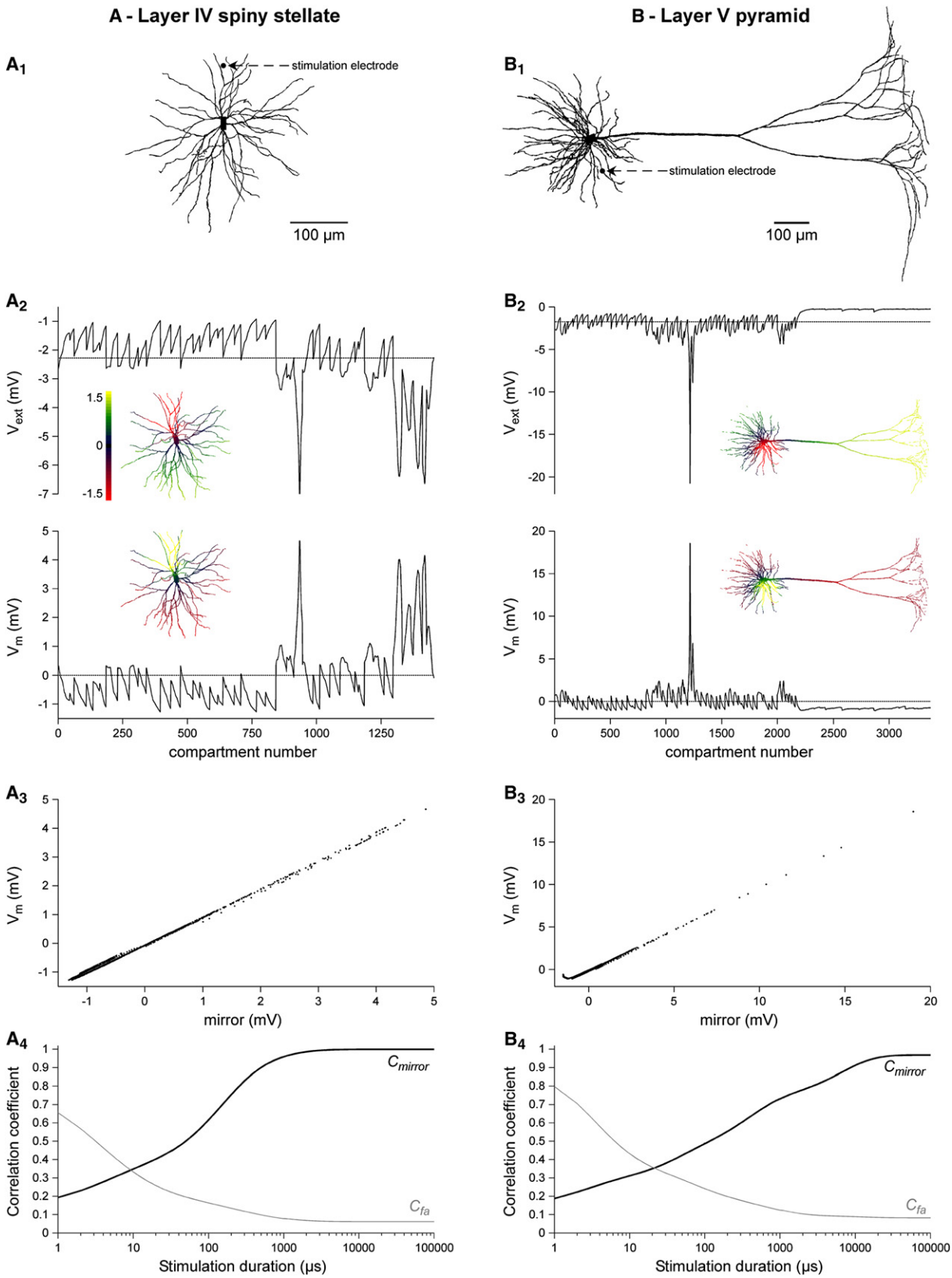

FIGURE 7 From the activating function to the mirror estimate: case of realistic cortical neurons. Realistic compartmentalized morphologies of cat visual cortex neurons are considered (a layer IV spiny stellate in A_1, a layer V pyramid in B_1, both taken from the literature (43)). In both cases, a cathodic stimulation (-1 μA) was delivered by a point-source electrode (*black point*) located at 100 μm from the soma. Only the passive responses of the cells were considered. The

in practice. As a rule of thumb, we found that the mirror estimate reaches a 99% matching with the actual steady-state solution for space constant values >25% of the fiber length (Fig. 5 *A*).

The purpose of this study was not to provide an exact prediction of the membrane potential profile during stimulation, but really to propose another intuitive estimate when the activating function was not adequate to predict membrane polarization. For this reason, we found interesting to examine the evolution of the frontier value (λ_f), above which the mirror estimator best predicts the membrane potential profile. Although the mirror domain is wider than the domain of parameters leading to a perfect match (e.g., >99%) between V_m and the mirror profile, it should be noted that, at the frontier between the two domains, the matching criterion is within the range 50%–92%. Moreover, the mirror approximation improves for increasing space constants and increasing stimulus durations. For instance, for our reference configuration and for space constants higher than 200 μm, C_{mirror} is 65% at the frontier (for a stimulation duration of 18 μs) and exceeds 88% as soon as the stimulation lasts more than 200 μs (Fig. 4), which corresponds to typical experimental situations.

Previous activating function studies (3,5,20) have dealt mainly with electrode-fiber distances of the order of 1 mm, and it has been pointed out previously that the activating function fails to accurately predict the membrane polarization for short distances of the order of 50 μm (8,18,39). Here, we spanned a wide range of distances, including smaller distances (down to 10 μm), which are likely to occur when using microelectrode arrays in direct contact with a neural tissue, either in vitro or in vivo. We found that the electrode-fiber distance has in fact a strong influence on the frontier between the mirror and activating function domains (Fig. 6). In particular, for typical space constants encountered in practice (>50–100 μm; Figs. 5 and 6), the mirror estimate is always more suitable for long distances ($> 0.23\times L$) irrespective of stimulus duration or fiber length, and also for short distances (<20–30 μm) when stimulus durations exceed a few tens of microseconds. For intermediate distances, the mirror estimate is all the more valid that the stimulus duration is long and the fiber is small (typically, for 100-μs pulses, the mirror estimate is best for fiber lengths <600 μm). Indeed, as shown in Fig. 6, for a given fiber length and stimulus duration, there is a restricted range of intermediate distances for which the activating function is the best predictor. This range shrinks and even disappears when either the stimulation duration or the fiber length increases.

Interestingly, the mirror estimate was found to be a good predictor of the membrane polarization at the steady state for realistic CNS neural morphologies with passive properties (Fig. 7). It can be seen that the mirror predictor is all the more valid for small stimulus durations that the morphology is compact. This simple estimate may thus be useful for the design of specific microstimulation paradigms and devices (such as dedicated microelectrode arrays) to achieve the activation of specific regions of neural arborizations in particular cortical layers or other regions of the CNS.

Although this study focused on unmyelinated fibers, we may predict that the mirror estimate would still be valid in the myelinated case. From intracellular or patch-clamp recordings of myelinated spinal motoneuron (47,48) and hippocampal pyramidal neurons and interneurons (49–51), space constant values can be estimated to be of the order of 55–2000 μm for a 1-μm-diameter fiber. However, these experimental values do not take into account the non homogeneity of node/internode space constants along the axon, which is likely to affect the equivalent space constant. Indeed, for myelinated axons, the node space constant is of the order of $\lambda_1 = 20$ μm, whereas the internode space constant λ_2 is usually considered 30-fold larger (12,16,42). Modeling studies (11,52) have shown that a myelinated fiber can be accurately approximated by a uniform fiber of equivalent space constant λ given by:

$$\lambda = \sqrt{\frac{(l_1 + l_2) \times \lambda_1^2 \times \lambda_2^2}{l_1 \times \lambda_2^2 + l_2 \times \lambda_1^2}},$$

where l_1 and l_2 stand for the node and internode lengths, respectively. Thus, for $l_1 = 1$ μm, $l_2 = 200$ μm, $\lambda_1 = 20$ μm, and $\lambda_2 = 600$ μm, one finds a typical equivalent unmyelinated space constant of 256 μm. It is thus expected that the mirror estimate remains valid for a large class of myelinated fibers.

In conclusion, these results show that the mirror estimate can be intuitively used to predict membrane polarization as an alternative to the activating function for a wide range of parameters corresponding to many situations encountered in practice.

APPENDIX

In this appendix, we derive the mirror approximation in the case of a nonuniform fiber (Eq. 11). We consider the case where the fiber diameter and the leakage conductance are different for each compartment k. Equation 1 can then be rewritten as:

induced extracellular potential field stimulation V_{ext} and the steady-state membrane potential V_m are plotted as a function of the compartment number (A_2, B_2). Insets show color-coded representations of $V_{ext} - \langle V_{ext} \rangle$ (*top*) and of the membrane polarization (*bottom*) for comparison with respect to the morphology. (A_3 and B_3) Same data plotted one against the other. In both cases, the steady-state membrane potential follows the mirror estimate very closely ($C_{mirror} = 1.00$ in A_3, $C_{mirror} = 0.97$ in B_3). Finally, A_4 and B_4 show the evolution of both matching criteria C_{mirror} and C_{fa} as a function of the stimulus duration for each cell. These plots show that the mirror estimate gives a better prediction of the membrane potential than the activating function estimate as long as the stimulation duration exceeds a few tens of microseconds.

$$C_{\mathrm{m}}^{(k)} \times \frac{dV_{\mathrm{m}}^{(k)}}{dt} + G_{\mathrm{l}}^{(k)} \times V_{\mathrm{m}}^{(k)} - \frac{V_{\mathrm{m}}^{(k-1)} - V_{\mathrm{m}}^{(k)}}{R^{(k,k-1)}} - \frac{V_{\mathrm{m}}^{(k+1)} - V_{\mathrm{m}}^{(k)}}{R^{(k,k+1)}} = \frac{V_{\mathrm{ext}}^{(k-1)} - V_{\mathrm{ext}}^{(k)}}{R^{(k,k-1)}} + \frac{V_{\mathrm{ext}}^{(k+1)} - V_{\mathrm{ext}}^{(k)}}{R^{(k,k+1)}}. \quad \text{(A1)}$$

Dividing both left- and right-hand sides of Eq. A1 by G_{l} and defining the membrane time constant of compartment k as $\tau^{(\mathrm{k})} = C_{\mathrm{m}}{}^{(\mathrm{k})}/G_{\mathrm{l}}{}^{(\mathrm{k})}$ leads to:

$$\tau^{(k)} \times \frac{dV_{\mathrm{m}}^{(k)}}{dt} + V_{\mathrm{m}}^{(k)} - \frac{V_{\mathrm{m}}^{(k-1)} - V_{\mathrm{m}}^{(k)}}{G_{\mathrm{l}}^{(k)} \times R^{(k,k-1)}} - \frac{V_{\mathrm{m}}^{(k+1)} - V_{\mathrm{m}}^{(k)}}{G_{\mathrm{l}}^{(k)} \times R^{(k,k+1)}} = \frac{V_{\mathrm{ext}}^{(k-1)} - V_{\mathrm{ext}}^{(k)}}{G_{\mathrm{l}}^{(k)} \times R^{(k,k-1)}} + \frac{V_{\mathrm{ext}}^{(k+1)} - V_{\mathrm{ext}}^{(k)}}{G_{\mathrm{l}}^{(k)} \times R^{(k,k+1)}}. \quad \text{(A2)}$$

One can derive an approximation of the $G_{\mathrm{l}}{}^{(\mathrm{k})} \times R^{(\mathrm{k},\mathrm{k}\pm1)}$ terms for a sufficiently fine discretization of the fiber. By definition,

$$G_{\mathrm{l}}^{(k)} \times R^{(k,k\pm1)} = \frac{1}{2} \times G_{\mathrm{l}}^{(k)} \times \left(R^{(k)} + R^{(k\pm1)}\right),$$

and, including surface and linear variables,

$$G_{\mathrm{l}}^{(k)} \times R^{(k,k\pm1)} = \frac{1}{2} \times g_{\mathrm{l}}^{(k)} \times \pi \times d^{(k)} \times \Delta s \times \left(\frac{4 \times \rho_{\mathrm{i}} \times \Delta s}{\pi \times d^{(k)2}} + \frac{4 \times \rho_{\mathrm{i}} \times \Delta s}{\pi \times d^{(k\pm1)2}}\right) = 2 \times g_{\mathrm{l}}^{(k)} \times \rho_{\mathrm{i}} \times \Delta s^2 \times \left(\frac{1}{d^{(k)}} + \frac{d^{(k)}}{d^{(k\pm1)2}}\right). \quad \text{(A3)}$$

Writing $d^{(k\pm1)} = d^{(\mathrm{k})} \pm \delta d^{(\mathrm{k})}$ and assuming a fine enough discretization so that $\delta d^{(\mathrm{k})} \ll d^{(\mathrm{k})}$ for any compartment k, the diameter of compartment $k \pm 1$ can be approximated by $d^{(\mathrm{k})}$ at the zeroth order. Equation A3 then leads to:

$$G_{\mathrm{l}}^{(k)} \times R^{(k,k\pm1)} = \frac{4 \times \rho_{\mathrm{i}} \times g_{\mathrm{l}}^{(k)}}{d^{(k)}} \times \Delta s^2 = \frac{\Delta s^2}{\lambda^{(k)2}}, \quad \text{(A4)}$$

by definition of the space constant of compartment k. Replacing Eq. A4 into Eq. A2 results in a modified cable equation similar to Eq. 2 of the theoretical section:

$$\tau^{(k)} \times \frac{dV_{\mathrm{m}}^{(k)}}{dt} + V_{\mathrm{m}}^{(k)} - \lambda^{(k)2} \times \frac{V_{\mathrm{m}}^{(k-1)} - 2 \times V_{\mathrm{m}}^{(k)} + V_{\mathrm{m}}^{(k+1)}}{\Delta s^2} = \lambda^{(k)2} \times \frac{V_{\mathrm{ext}}^{(k-1)} - 2 \times V_{\mathrm{ext}}^{(k)} + V_{\mathrm{ext}}^{(k+1)}}{\Delta s^2}. \quad \text{(A5)}$$

Similarly, boundary equations can be derived as follows:

$$\tau^{(0)} \times \frac{dV_{\mathrm{m}}^{(0)}}{dt} + V_{\mathrm{m}}^{(0)} - \lambda^{(0)2} \times \frac{-V_{\mathrm{m}}^{(0)} + V_{\mathrm{m}}^{(1)}}{\Delta s^2} = \lambda^{(0)2} \times \frac{-V_{\mathrm{ext}}^{(0)} + V_{\mathrm{ext}}^{(1)}}{\Delta s^2}, \quad \text{(A6a)}$$

$$\tau^{(\mathrm{N})} \times \frac{dV_{\mathrm{m}}^{(\mathrm{N})}}{dt} + V_{\mathrm{m}}^{(\mathrm{N})} - \lambda^{(\mathrm{N})2} \times \frac{-V_{\mathrm{m}}^{(\mathrm{N})} + V_{\mathrm{m}}^{(\mathrm{N}-1)}}{\Delta s^2} = \lambda^{(\mathrm{N})2} \times \frac{-V_{\mathrm{ext}}^{(\mathrm{N})} + V_{\mathrm{ext}}^{(\mathrm{N}-1)}}{\Delta s^2}. \quad \text{(A6b)}$$

Following the same reasoning as the one detailed for a uniform fiber (see the theoretical section), we derive a simple and general steady-state analytical solution to the system of Eqs. A5 and A6 in the case where all $\lambda^{(\mathrm{k})}$ are large enough. From Eq. A5, the membrane potential is approximated by the following expression:

$$V_{\mathrm{m}}^{(k)} = -V_{\mathrm{ext}}^{(k)} + c_1 \times k \times \Delta s + c_2. \quad \text{(A7)}$$

Inserting Eq. A7 into one of the boundary equations A6a or A6b, leads to $c_1 = 0$. Furthermore, at the steady state, Eqs. A5 and A6 can be written as:

$$\frac{V_{\mathrm{m}}^{(k)}}{\lambda^{(k)2}} - \frac{V_{\mathrm{m}}^{(k-1)} - 2 \times V_{\mathrm{m}}^{(k)} + V_{\mathrm{m}}^{(k+1)}}{\Delta s^2} = \frac{V_{\mathrm{ext}}^{(k-1)} - 2 \times V_{\mathrm{ext}}^{(k)} + V_{\mathrm{ext}}^{(k+1)}}{\Delta s^2}$$

$$\frac{V_{\mathrm{m}}^{(0)}}{\lambda^{(0)2}} - \frac{-V_{\mathrm{m}}^{(0)} + V_{\mathrm{m}}^{(1)}}{\Delta s^2} = \frac{-V_{\mathrm{ext}}^{(0)} + V_{\mathrm{ext}}^{(1)}}{\Delta s^2}$$

$$\frac{V_{\mathrm{m}}^{(\mathrm{N})}}{\lambda^{(\mathrm{N})2}} - \frac{-V_{\mathrm{m}}^{(\mathrm{N})} + V_{\mathrm{m}}^{(\mathrm{N}-1)}}{\Delta s^2} = \frac{-V_{\mathrm{ext}}^{(\mathrm{N})} + V_{\mathrm{ext}}^{(\mathrm{N}-1)}}{\Delta s^2}$$

Summing all equations of this system leads to:

$$\sum_{k=0}^{\mathrm{N}} \frac{V_{\mathrm{m}}^{(k)}}{\lambda^{(k)2}} = 0, \quad \text{(A8)}$$

which generalizes Eq. 7 obtained in the uniform case. Finally, introducing Eq. A7 into Eq. A8 leads to:

$$c_2 = \sum_{k=0}^{\mathrm{N}} \frac{V_{\mathrm{ext}}^{(k)}}{\lambda^{(k)2}} \Bigg/ \sum_{k=0}^{\mathrm{N}} \frac{1}{\lambda^{(k)2}}. \quad \text{(A9)}$$

In conclusion, in the (general) non uniform case, assuming that all $\lambda^{(\mathrm{k})}$ are large enough, the membrane potential is the mirror of the extracellular potential centered on its spatial mean value weighted by the squared inverse of the space constants:

$$V_{\mathrm{m}}^{(k)} = -V_{\mathrm{ext}}^{(k)} + \sum_{\mathrm{j}=0}^{\mathrm{N}} \frac{V_{\mathrm{ext}}^{(\mathrm{j})}}{\lambda^{(\mathrm{j})2}} \Bigg/ \sum_{\mathrm{j}=0}^{\mathrm{N}} \frac{1}{\lambda^{(\mathrm{j})2}}, \quad \text{(A10)}$$

which becomes, in the continuous case:

$$V_m(s) = -V_{ext}(s) + \int_{s=-\frac{L}{2}}^{\frac{L}{2}} \frac{V_{ext}(s)}{\lambda(s)^2}\,ds \Bigg/ \int_{s=-\frac{L}{2}}^{\frac{L}{2}} \frac{1}{\lambda(s)^2}\,ds. \tag{A11}$$

The authors thank D. Cattaert for fruitful discussions.

This work was supported by the French ministry for research and technology (RMNT Neurocom project No. 03J489 and ACI Neurosciences Intégratives et Computationnelles No 2003541), the French National Research Agency (ANR-Programme Blanc No ANR06BLAN035601 and Programme TecSan No ANR07TECSAN01404), the Fyssen and Medical Research (FRM) foundations (Paris), the Institut pour la Recherche sur la Moelle Epinière et l'Encéphale (IRME), and the Région Aquitaine (20030301201A and 20040301202A).

REFERENCES

1. Ranck, Jr., J. B. 1975. Which elements are excited in electrical stimulation of mammalian central nervous system: a review. *Brain Res.* 98:417–440.
2. McNeal, D. R. 1976. Analysis of a model for excitation of myelinated nerve. *IEEE Trans. Biomed. Eng.* 23:329–337.
3. Rattay, F. 1986. Analysis of models for external stimulation of axons. *IEEE Trans. Biomed. Eng.* 33:974–977.
4. Rubinstein, J. T., and F. A. Spelman. 1988. Analytical theory for extracellular electrical stimulation of nerve with focal electrodes. I. Passive unmyelinated axon. *Biophys. J.* 54:975–981.
5. Rattay, F. 1989. Analysis of models for extracellular fiber stimulation. *IEEE Trans. Biomed. Eng.* 36:676–682.
6. Coburn, B. 1989. Neural modeling in electrical stimulation. *Crit. Rev. Biomed. Eng.* 17:133–178.
7. Altman, K. W., and R. Plonsey. 1990. Point source nerve bundle stimulation: effects of fiber diameter and depth on simulated excitation. *IEEE Trans. Biomed. Eng.* 37:688–698.
8. Altman, K. W., and R. Plonsey. 1990. Analysis of excitable cell activation: relative effects of external electrical stimuli. *Med. Biol. Eng. Comput.* 28:574–580.
9. Roth, B. J., and P. J. Basser. 1990. A model of the stimulation of a nerve fiber by electromagnetic induction. *IEEE Trans. Biomed. Eng.* 37: 588–597.
10. Basser, P. J., and B. J. Roth. 1991. Stimulation of a myelinated nerve axon by electromagnetic induction. *Med. Biol. Eng. Comput.* 29:261–268.
11. Rubinstein, J. T. 1991. Analytical theory for extracellular electrical stimulation of nerve with focal electrodes. II. Passive myelinated axon. *Biophys. J.* 60:538–555.
12. Warman, E. N., W. M. Grill, and D. Durand. 1992. Modeling the effects of electric fields on nerve fibers: determination of excitation thresholds. *IEEE Trans. Biomed. Eng.* 39:1244–1254.
13. Struijk, J. J., J. Holsheimer, G. G. van der Heide, and H. B. Boom. 1992. Recruitment of dorsal column fibers in spinal cord stimulation: influence of collateral branching. *IEEE Trans. Biomed. Eng.* 39: 903–912.
14. Struijk, J. J., J. Holsheimer, and H. B. Boom. 1993. Excitation of dorsal root fibers in spinal cord stimulation: a theoretical study. *IEEE Trans. Biomed. Eng.* 40:632–639.
15. Nagarajan, S. S., D. M. Durand, and E. N. Warman. 1993. Effects of induced electric fields on finite neuronal structures: a simulation study. *IEEE Trans. Biomed. Eng.* 40:1175–1188.
16. Rubinstein, J. T. 1993. Axon termination conditions for electrical stimulation. *IEEE Trans. Biomed. Eng.* 40:654–663.
17. Roth, B. J. 1994. Mechanisms for electrical stimulation of excitable tissue. *Crit. Rev. Biomed. Eng.* 22:253–305.
18. Plonsey, R., and R. C. Barr. 1995. Electric field stimulation of excitable tissue. *IEEE Trans. Biomed. Eng.* 42:329–336.
19. Plonsey, R., and R. C. Barr. 1998. Electric field stimulation of excitable tissue. *IEEE Eng. Med. Biol. Mag.* 17:130–137.
20. Rattay, F. 1999. The basic mechanism for the electrical stimulation of the nervous system. *Neuroscience.* 89:335–346.
21. McIntyre, C. C., and W. M. Grill. 1999. Excitation of central nervous system neurons by nonuniform electric fields. *Biophys. J.* 76:878–888.
22. Basser, P. J., and B. J. Roth. 2000. New currents in electrical stimulation of excitable tissues. *Annu. Rev. Biomed. Eng.* 2:377–397.
23. Schnabel, V., and J. J. Struijk. 2001. Evaluation of the cable model for electrical stimulation of unmyelinated nerve fibers. *IEEE Trans. Biomed. Eng.* 48:1027–1033.
24. McIntyre, C. C., and W. M. Grill. 2002. Extracellular stimulation of central neurons: influence of stimulus waveform and frequency on neuronal output. *J. Neurophysiol.* 88:1592–1604.
25. McIntyre, C. C., W. M. Grill, D. L. Sherman, and N. V. Thakor. 2004. Cellular effects of deep brain stimulation: model-based analysis of activation and inhibition. *J. Neurophysiol.* 91:1457–1469.
26. Lertmanorat, Z., and D. M. Durand. 2004. A novel electrode array for diameter-dependent control of axonal excitability: a simulation study. *IEEE Trans. Biomed. Eng.* 51:1242–1250.
27. Lertmanorat, Z., and D. M. Durand. 2004. Extracellular voltage profile for reversing the recruitment order of peripheral nerve stimulation: a simulation study. *J. Neural Eng.* 1:202–211.
28. Mino, H., J. T. Rubinstein, C. A. Miller, and P. J. Abbas. 2004. Effects of electrode-to-fiber distance on temporal neural response with electrical stimulation. *IEEE Trans. Biomed. Eng.* 51:13–20.
29. Vuckovic, A., N. J. Rijkhoff, and J. J. Struijk. 2004. Different pulse shapes to obtain small fiber selective activation by anodal blocking–a simulation study. *IEEE Trans. Biomed. Eng.* 51:698–706.
30. Manola, L., B. H. Roelofsen, J. Holsheimer, E. Marani, and J. Geelen. 2005. Modelling motor cortex stimulation for chronic pain control: electrical potential field, activating functions and responses of simple nerve fibre models. *Med. Biol. Eng. Comput.* 43:335–343.
31. Manola, L., J. Holsheimer, P. Veltink, and J. R. Buitenweg. 2007. Anodal vs. cathodal stimulation of motor cortex: a modeling study. *Clin. Neurophysiol.* 118:464–474.
32. Plonsey, R. 1969. Bioelectric Phenomena. McGraw-Hill, New York.
33. Church, P., A. Leduc, R. A. Beique, and J. R. Derome. 1984. A numerical solution of cylindrical coordinate Laplace's equation with mixed boundary conditions along the axis of symmetry: application to intracerebral stimulating electrodes. *J. Appl. Phys.* 56:1–5.
34. Fromherz, P. 2002. Sheet conductor model of brain slices for stimulation and recording with planar electronic contacts. *Eur. Biophys. J.* 31:228–231.
35. Struijk, J. J., J. Holsheimer, B. K. van Veen, and H. B. Boom. 1991. Epidural spinal cord stimulation: calculation of field potentials with special reference to dorsal column nerve fibers. *IEEE Trans. Biomed. Eng.* 38:104–110.
36. McIntyre, C. C., and W. M. Grill. 2001. Finite element analysis of the current-density and electric field generated by metal microelectrodes. *Ann. Biomed. Eng.* 29:227–235.
37. Joucla, S., and B. Yvert. 2009. Improved focalization of electrical microstimulation using microelectrode arrays: a modeling study. *PLoS ONE.* 4:e4828.
38. Knisley, S. B. 2000. Evidence for roles of the activating function in electric stimulation. *IEEE Trans. Biomed. Eng.* 47:1114–1119.
39. Zierhofer, C. M. 2001. Analysis of a linear model for electrical stimulation of axons–critical remarks on the "activating function concept". *IEEE Trans. Biomed. Eng.* 48:173–184.
40. Dayan, P., and L. F. Abbott. 2001. Theoretical Neuroscience. MIT Press, Cambridge, Massachusetts.

41. Hines, M. L., and N. T. Carnevale. 1997. The NEURON simulation environment. *Neural Comput.* 9:1179–1209.

42. Mainen, Z. F., J. Joerges, J. R. Huguenard, and T. J. Sejnowski. 1995. A model of spike initiation in neocortical pyramidal neurons. *Neuron.* 15:1427–1439.

43. Mainen, Z. F., and T. J. Sejnowski. 1996. Influence of dendritic structure on firing pattern in model neocortical neurons. *Nature.* 382:363–366.

44. Sobie, E. A., R. C. Susil, and L. Tung. 1997. A generalized activating function for predicting virtual electrodes in cardiac tissue. *Biophys. J.* 73:1410–1423.

45. Altman, K. W., and R. Plonsey. 1988. Development of a model for point source electrical fibre bundle stimulation. *Med. Biol. Eng. Comput.* 26:466–475.

46. Jean-Xavier, C., G. Z. Mentis, M. J. O'Donovan, D. Cattaert, and L. Vinay. 2007. Dual personality of GABA/glycine-mediated depolarizations in immature spinal cord. *Proc. Natl. Acad. Sci. USA.* 104:11477–11482.

47. Barrett, J. N., and W. E. Crill. 1974. Specific membrane properties of cat motoneurons. *J. Physiol.* 239:301–324.

48. Fleshman, J. W., I. Segev, and R. B. Burke. 1988. Electrotonic architecture of type-identified alpha-motoneurons in the cat spinal cord. *J. Neurophysiol.* 60:60–85.

49. Turner, D. A., and P. A. Schwartzkroin. 1983. Electrical characteristics of dendrites and dendritic spines in intracellularly stained CA3 and dentate hippocampal neurons. *J. Neurosci.* 3:2381–2394.

50. Turner, D. A., and P. A. Schwartzkroin. 1980. Steady-state electrotonic analysis of intracellularly stained hippocampal neurons. *J. Neurophysiol.* 44:184–199.

51. Spruston, N., D. B. Jaffe, and D. Johnston. 1994. Dendritic attenuation of synaptic potentials and currents: the role of passive membrane properties. *Trends Neurosci.* 17:161–166.

52. Andrietti, F., and G. Bernardini. 1984. Segmented and "equivalent" representation of the cable equation. *Biophys. J.* 46:615–623.